# Synthesis, Characterization, and Biological Properties of Steroidal Ruthenium(II) and Iridium(111) Complexes Based on the Androst-16-en-3-ol Framework

Koch, Vanessa

2019-12-02

Koch , V , Meschkov , A , Feuerstein , W , Pfeifer , J , Fuhr , O , Nieger , M , Schepers , U & Bräse , S 2019 , ' Synthesis, Characterization, and Biological Properties of Steroidal Ruthenium(II) and Iridium(111) Complexes Based on the Androst-16-en-3-ol Framework ' , Inorganic Chemistry , vol. 58 , no. 23 , pp. 15917-15926 . https://doi.org/10.1021/acs.inorgchem.9b02402

http://hdl.handle.net/10138/321395
https://doi.org/10.1021/acs.inorgchem.9b02402

unspecified
acceptedVersion

# Synthesis, characterization and biological properties of novel steroidal ruthenium(II) and iridium(III) complexes based on the androst-16-en-3-ol framework

| | |
|---|---|
| Journal: | *Inorganic Chemistry* |
| Manuscript ID | Draft |
| Manuscript Type: | Article |
| Date Submitted by the Author: | n/a |
| Complete List of Authors: | Koch, Vanessa; Karlsruher Institut fur Technologie, Chemistry<br>Meschkov, Anna; Karlsruher Institut fur Technologie, Institute of Functional Interfaces<br>Feuerstein, Wolfram; Karlsruher Institut fur Technologie, Chemistry<br>Fuhr, Olaf; Karlsruher Institut für Technologie, Institut für Nanotechnologie<br>Nieger, Martin; University of Helsinki<br>Schepers, Ute; Karlsruher Institut fur Technologie - Campus Nord, Institute of Functional Interfaces<br>Bräse, Stefan; Karlsruher Institut fur Technologie, Chemistry |
| | |

# Synthesis, characterization and biological properties of novel steroidal ruthenium(II) and iridium(III) complexes based on the androst-16-en-3-ol framework

Vanessa Koch[a], Anna Meschkov[a,b], Wolfram Feuerstein[c], Olaf Fuhr[d], Martin Nieger[e], Ute Schepers[a,b], Stefan Bräse[a,f]*

a Institute of Organic Chemistry (IOC), Karlsruhe Institute of Technology (KIT), Fritz-Haber-Weg 6, 76131 Karlsruhe, Germany. Fax: (+49)-721-6084-8581; phone: (+49)-721-6084-2903; e-mail: braese@kit.edu.

b Institute of Functional Interfaces (IFG), Karlsruhe Institute of Technology (KIT), Hermann von Helmholtz Platz 1, 76344 Eggenstein-Leopoldshafen, Germany

c Institute of Inorganic Chemistry, Division Molecular Chemistry, Karlsruhe Institute of Technology (KIT), Engesserstr. 15, 76131 Karlsruhe (Germany).

d Institute for Nanotechnology (INT) and Karlsruhe Nano Micro Facility (KNMF), Karlsruhe Institute of Technology (KIT), Hermann von Helmholtz Platz 1, 76344 Eggenstein-Leopoldshafen, Germany

e Department of Chemistry, University of Helsinki, P. O. Box 55, 00014 University of Helsinki, Finland.

f Institute of Toxicology and Genetics, Karlsruhe Institute of Technology (KIT), Hermann-von-Helmholtz-Platz 1, D-76344 Eggenstein-Leopoldshafen, Germany.

Steroids, metallocycle, ruthenium(II), iridium(III)

**Abstract**

A range of novel cyclometalated ruthenium(II) and iridium(III) complexes with a steroidal backbone based on androsterone were synthesized and characterized by NMR spectroscopy and X-ray crystallography. Their cytotoxic properties in both RT112 and RT112cp (cisplatin-resistant) cell lines were compared with those of the corresponding non-steroidal complexes and the non-cyclometalated pyridyl complexes as well as with cisplatin as reference. All steroidal complexes were more active in RT112cp cells than cisplatin whereby the cyclometalated pyridinylphenyl complexes based on **5c** showed high cytotoxicity (**7**: $LD_{50}$ 3 μM for RT112 and 1 μM for

RT112cp; **10**: $LD_{50}$ 2 μM for RT112 and 1 μM for RT112cp) while maintaining low resistant factors of 0.33 and 0.50.

**Author Contributions**

The manuscript was written through contributions of all authors. All authors have given approval to the final version of the manuscript.

## Introduction

Over the past 60 years the interest in steroid-bearing transition-metal complexes has increased continuously.[1] In the late 1970s, the biological application of these complexes was discovered enabling new perspectives for metal-containing approaches e.g., in the treatment of cancer.[1] Although platinum-based anticancer complexes[2] such as cisplatin[3] or oxaliplatin[4] are worldwide recognized for the treatment of cancer, still some drawbacks remain. In order to circumvent intrinsic and acquired resistance and to reduce side effects, other transition-metal based anticancer agents have been explored.[5] Based on ruthenium(III), KP1019[6] and NAMI-A[7] (Figure 1) were developed, whereby both drugs already passed phase I of the clinical trials[8]. Ruthenium(III) probably serves as a pro-drug and is reduced within the cell to the active ruthenium(II) complex. Noteworthy, ruthenium complexes of the type [Ru($\eta^6$-arene)$Cl_2$(PTA)] (PTA = 1,3,5-triaza-7-phosphatricyclo-[3.3.1.1]decane) also show promising anticancer properties and are therefore broadly investigated.[9] By connecting the metal center to a steroidal backbone as shown in complex **1** and **2** (Figure 1), biological properties can be tuned. Since the steroidal framework enables the binding to steroid receptors, cell penetration can be improved. It has been also demonstrated that by the incorporation of a C-3 modified cholesterol ruthenium(III) complex **2** into a liposome bilayer, the ruthenium moiety was protected from degradation and the cellular uptake was favored. When integrated into a biomimetic membrane, the complex was found to be 6-fold times more active against MCF-7 cell lines (breast cancer) than the corresponding non-steroidal complex.[10] Moreover, Jaouen[11] and later Hannon[12] could show that a sufficient recognition of steroidal receptors is retained if the organometallic site is attached at the end of a rigid spacer such as an ethynyl group at C-17 of an estradiol or testosterone derivative. In this

context, Ruiz *et al*. found that the androgen-containing ruthenium(II) complexes **1** was 8-fold more active than cisplatin in T47D cell lines (breast cancer).[13]

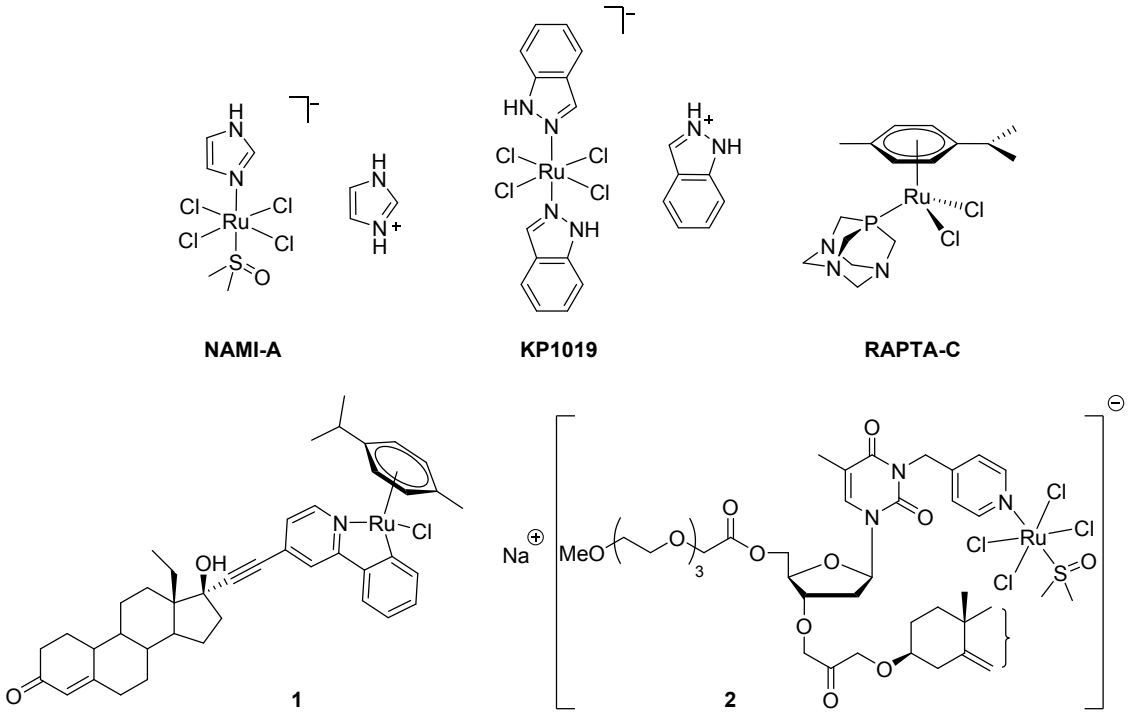


**Figure 1:** Currently investigated Ru(III)- and Ru(II)-anticancer drugs and ruthenium complexes based on an androgen (**1**) and a cholesterol (**2**) framework.

Compared to the number of studies on the anticancer activity of ruthenium complexes, only a few reports regarding the anticancer activity of iridium(III) complexes have been published.[13a, 14] Nevertheless, Sadler *et al.* showed that the biological activity of pentamethylcyclopentadienyl ($Cp^*$)Ir(III) complexes was increased by the incorporation of phenyl substituents. This resulted in an enhanced cellular accumulation due to the higher hydrophobicity of these complexes. Furthermore, the substitution of *N*,*N*-ligands by *C*,*N*-chelating ligands was shown to improve antiproliferative activity.

Motivated by these results, we envisioned to investigate the chemical, spectroscopic and biological properties of novel ruthenium(II) and iridium(III) complexes based on *epi*-androsterone with the metal center located closer to the steroidal backbone compared to previous examples.[13]

**Design and Synthesis of the New Ruthenium Complexes**

In order to bring the steroidal backbone in close proximity to the metal center, we aimed to modify C-17 of *epi*-androsterone (**3**) in such a manner that the complexation of ruthenium(II) and the iridium(III) is feasible either by a *N*-pyridine moiety or by $\kappa^2$-*N*,*C*-cyclometalation. Therefore, different pyridine substituted androsterone derivatives (**5a**, **5b**) and a 4′-(2-pyridinyl)phenyl derivative (**5c**) were synthesized. As previously shown by our group, pyridine containing substituents are best introduced by the Stille cross-coupling reaction.[15] Starting from *epi*-androsterone (**3**), the desired ligands were easily accessible by a two-step procedure (Scheme 1). Hence, *epi*-androsterone (**3**) was treated with hydrazine to form the hydrazone giving either the alkenyl iodide **4a** by adding iodine in the presence of triethylamine or the alkenyl bromide **4b** by adding NBS with pyridine as base. The following palladium-catalyzed Stille cross-coupling reaction afforded the 2′-pyridinyl derivative **5a**, 3′-pyridinyl derivative **5b**, or 4-(pyridin-2′-yl)phenyl derivative **5c** in good yields ranging from 60–74%. By washing the obtained products **5** with *n*-hexane, traces of remaining stannanes could be removed, which was crucial with regard to biological tests.

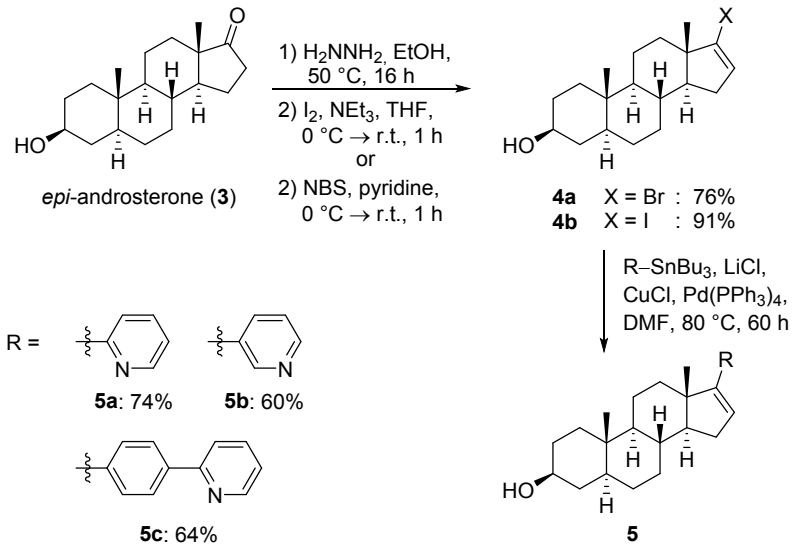


**Scheme 1:** Synthesis of the steroidal pyridine-containing ligands **5** starting from *epi*-androsterone (**3**) *via* a two-step procedure.[15]

Since numerous procedures exist in literature for the synthesis of cyclic ruthenium(II) complexes of 2-phenylpyridines,[16] we tried analogous reaction conditions with 2-(4-bromophenyl)pyridine. With one equivalent of dimeric ruthenium precursor $[Ru(\eta^6\text{-}para\text{-cymene})Cl_2]_2$ and two equivalents of the ligand in the presence of four equivalents of KOAc in MeOH, the Ru(II) complex was formed after stirring at r.t. for 24 h. After flash column chromatography on silica gel, the ruthenium(II) complex **6** was isolated with 67% yield (Scheme 2). Applying the same reaction conditions, the synthesis of the phenylpyridinyl ruthenium(II) complex **7** and the pyridinyl ruthenium(II) complex **8** succeeded in moderate yields starting from their ligands **5c** or **5a** (Scheme 2).

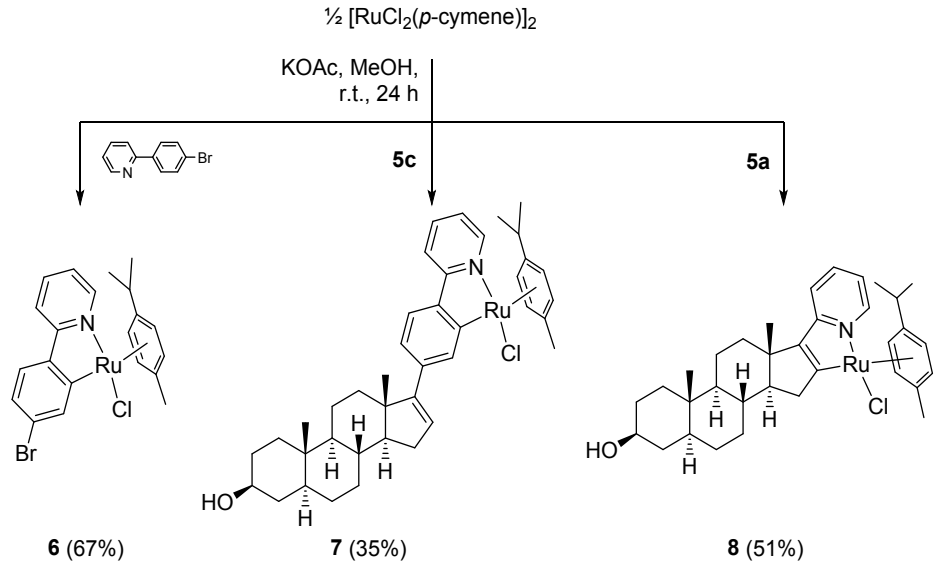


**Scheme 2:** Synthesis of novel cycloruthenated ruthenium(II) complexes **6**, **7** and **8**.

By recording $^{1}H$ and $^{13}C$ NMR, IR and FAB mass spectra the complexes **6**, **7** and **8** were successfully characterized. The Ru-metal takes a pseudo-tetrahedral "piano stool" coordination geometry generating a new stereogenic center. Hence, most of the NMR resonances of the pyridinylphenyl ruthenium(II) complex **7** in $d_1$-chloroform were duplicated (see Supporting Information). DFT calculations on the BP86[17]/def2-TZVPP[18] level reveal the two diastereomers to differ only 5.6 kJ/mol in Gibbs free energy. Accordingly, both diastereomers were formed in comparable amounts as evidenced by NMR signal intensities showing that no diastereomeric induction for cycloruthenation occurred. Furthermore, a single crystal suitable for X-ray crystallography was obtained confirming the stated molecular structure for the *R*-diastereomer as depicted in Figure 2. The coordination geometry of the Ru(II) center shows the expected pseudo-tetrahedral geometry. The N–Ru–C angle of 77.72° is significantly smaller than the N–Ru–Cl (86.98°) and the Cl–Ru–C (85.76°) angle which is in agreement with reported nonsteroidal cycloruthenated 2-phenylpyridinyl complexes[19]. In comparison with nonsteroidal complexes reported in the literature[19-20], ruthenium(II) complex **7** show similar bond angles and bond

lengths, whereby Ru–X bond lengths (X = N, Cl, C) are slightly longer and bond angles Y–Ru–Z (Y ≠ Z = N, Cl, C) slightly smaller. Unfortunately, we were not able to assign the crystal structure to one of the NMR signal sets, since the NMR chemical shifts of the diastereomers are too similar as predicted by NMR shielding calculations (see Supporting Information).

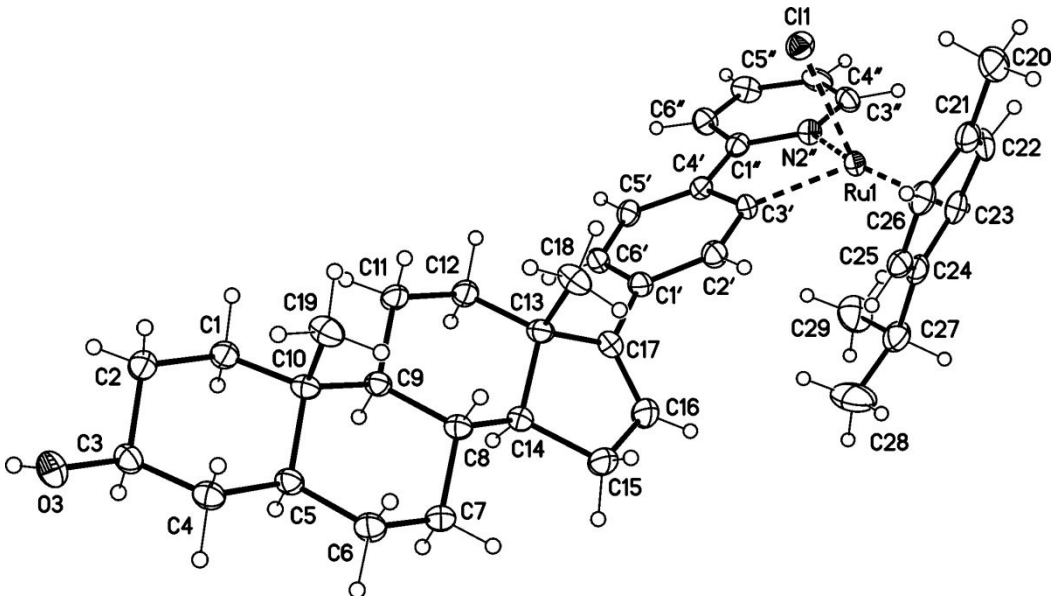


**Figure 2:** Molecular structure of the pyridylphenyl ruthenium(II) complex **7** (displacement parameters are drawn at 50% probability level). Characteristic bond lengths: Characteristic bond lengths: Ru–N 2.097(3) Å; Ru–C 2.047(3) Å; Ru–Cl 2.4253(7) Å; Ru–$C^{cymene}$ 2.154(3)–2.290(3) Å; Ru–$C^{cymene/centroid}$ 1.706(3) Å. Selected bond angles: N–Ru–C 77.72(12)°, N–Ru–Cl 86.98(3)°, Cl–Ru–C 85.76(9)°, N–Ru–$cymene^{centroid}$ 132.3(1)°, Cl–Ru–$cymene^{centroid}$ 126.6(1)°, C–Ru–$cymene^{centroid}$ 130.3(1)°.

Fortunately, in the case of the 2-pyridinyl ruthenium(II) complex **8**, the diastereomers could be separated by column chromatography on silica whereby both diastereomers **(*R*-Ru)-8** and **(*S*-**

**Ru)-8** were formed in equal amounts according to the integration of the crude $^{1}$H NMR spectrum and could be isolated in comparable amounts. As for complex **7**, by optimizing the molecular structures of both diastereomers on the BP86[17]/def2-TZVPP[18] level of theory we could show that none of the two diastereomers was noticeably thermodynamically favored standing in line with the nearly equimolar ratio of the isolated product. Both diastereomers showed nearly the same Gibbs free energies differing only in 3.2 kJ/mol in favor of the (*S*)-diastereomer. In addition, we calculated $^{1}$H and $^{13}$C NMR shifts employing different density functionals using the optimized structures of both diastereomers to be compared with the experimental resonances. The TPSSh functional[21] turned out to yield the best accordance with the experimental NMR shift differences between **(*R*-Ru)-8** and **(*S*-Ru)-8** (see Supporting Information). This allowed for the assignment of the obtained NMR spectra to the two diastereomers (Table 1).

**Table 1:** Experimental proton and carbon resonances of the diastereomers **(*R*-Ru)-8** and **(*S*-Ru)-8** and their experimental differences of the chemical shifts $\Delta_\delta = \delta_S - \delta_R$ as well as their differences $^{cal}\Delta_\delta = \delta_{(S)} - \delta_{(R)}$ calculated on the TPSSh/def2-TZVPP level of theory using bp86/def2-TZVPP structures. By comparing the calculated with experimental differences in chemical shifts, the diastereomers **(*R*-Ru)-8** and **(*S*-Ru)-8** were assigned. n.d. = not determined. See text for computational details.

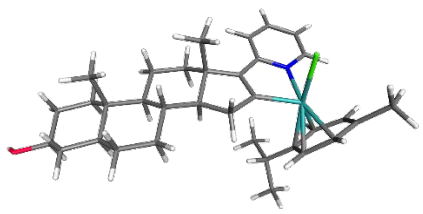

(*R*)-diastereomer

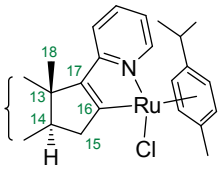


**8**

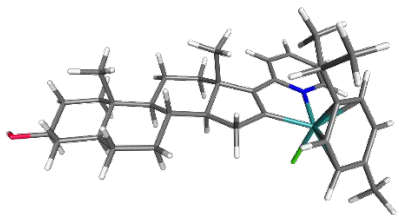

(*S*)-diastereomer

| | **$^{13}$C** | | | | **$^{1}$H** | | | |
|---|---|---|---|---|---|---|---|---|
| | $\delta_R$ [ppm] | $\Delta_\delta$ $_{(S-R)}$ [ppm] | $\delta_S$ [ppm] | $^{cal}\Delta_\delta$ [ppm] | $\delta_R$ [ppm] | $\Delta_\delta$ [ppm] | $\delta_S$ [ppm] | $^{cal}\Delta_\delta$ [ppm] |

| | | | | | | | | |
|---|---|---|---|---|---|---|---|---|
| 16-$C_q$–Ru | 208.7 | +1.0 | 209.7 | +0.6 | - | - | - | - |
| 17-$C_q$–Pyr | 150.4 | +0.3 | 150.7 | +0.2 | - | - | - | - |
| 13-$C_q$ | 44.8 | –0.5 | 44.3 | –0.2 | - | - | - | - |
| 18-$CH_3$ | 16.6 | +0.8 | 17.4 | +1.7 | 0.84 | +0.09 | 0.93 | +0.12 |
| 15$\alpha$-$CH_2$ | 44.8 | –0.5 | 44.3 | –0.3 | 3.11 | –0.13 | 2.98 | –0.25 |
| 15$\beta$-$CH_2$ | | | | | 2.50 | +0.34 | 2.84 | +0.33 |
| 14-CH | 58.5 | –0.2 | 58.3 | +1.1 | n.d. | n.d. | n.d. | –0.01 |

The corresponding $^1$H NMR spectra and the relevant assignments are depicted in Figure 3. The stacked NMR spectra show no differences in chemical shifts for the proton resonances of the pyridinyl moiety. The aromatic and aliphatic proton resonances of the cymene ligand on the other hand, were clearly shifted similar to the three isopropyl resonances of **(*S*-Ru)-8** that appear at lower chemical shifts compared to the ones of **(*R*-Ru)-8**. Also, the resonances of steroidal backbone close to the ruthenium center are affected by the different electronic environments of the two diastereomers. For example, in case of the diastereomer **(*R*-Ru)-8** the methyl group and the chlorido substituent were located on the same side resulting in a chemical shift of $\delta = 0.94$ ppm, while the resonances of the diastereomer **(*S*-Ru)-8** are shifted upfield to $\delta = 0.84$ ppm. Furthermore, the two diastereomeric 15-$CH_2$ resonances were influenced by the coordination to the pseudo-tetrahedral ruthenium center, whereby both signal sets were shifted downfield compared to those of the steroidal ligand **5b**. NOESY experiments and the evaluation of the coupling constants allowed the assignment of the more shielded signals to the 15$\beta$-$CH_2$ protons, while the signals that arise more downfield belong to the 15$\alpha$-$CH_2$ protons being in accordance with our calculations of the chemical shielding. It is noteworthy that for diastereomer **(*S*-Ru)-8**, the individual 15-$CH_2$ resonances were closer to each other than those for the diastereomer **(*R*-Ru)-8** which was predicted by our chemical shielding calculations as well. This behavior is caused by the chlorido substituent: The non-bonding electrons lead to a shielding of spatially close protons by $n$–$\sigma^*$ interactions.[22] Hence, the $\beta$-proton of diastereomer **(*R*-Ru)-8** is shifted to higher fields

compared to its **(*S*-Ru)-8** counterpart. The same held true for the $\alpha$-proton of **(*S*-Ru)-8**, which is however, less pronounced.

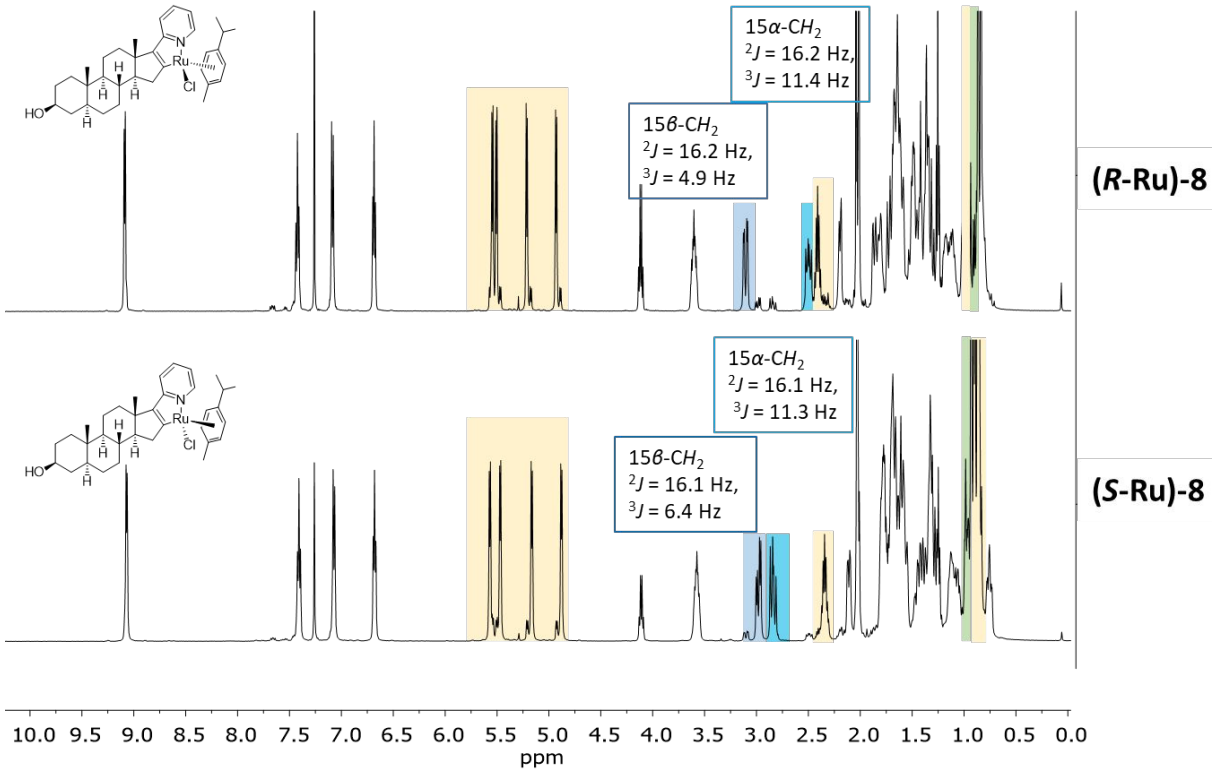


**Figure 3:** $^1$H NMR spectra ($CDCl_3$, 500 MHz, r.t.) of the diastereomers **(*R*-Ru)-8** (top) and **(*S*-Ru)-8** (bottom). Significantly different shifts of the two diastereomers are highlighted (blue: 15-$CH_2$, yellow: cymene, green = 18-$CH_3$).

We were able to obtain a crystal structure of the (*R*)-diastereomer of **8** (Figure 4) confirming the molecular structure and the correct assignments of the diastereomers based on the calculated chemical shifts. In contrast to the phenylpyridinyl ruthenium(II) complex **6** and its steroidal counterpart **7**, the Ru–C bond of **(*R*-Ru)-8** is significantly shorter (1.931 Å vs 2.062 Å of **6**[20]/ 2.047 Å of **7**). This is an indication for the inferior electron donating ability of the cyclopentenido moiety of the steroidal D-ring compared to phenyl. To the best of our knowledge, the herein

presented ruthenium complex **8** is the first example of a cyclopentenido-pyridinyl ruthenium(II) complex.[23]

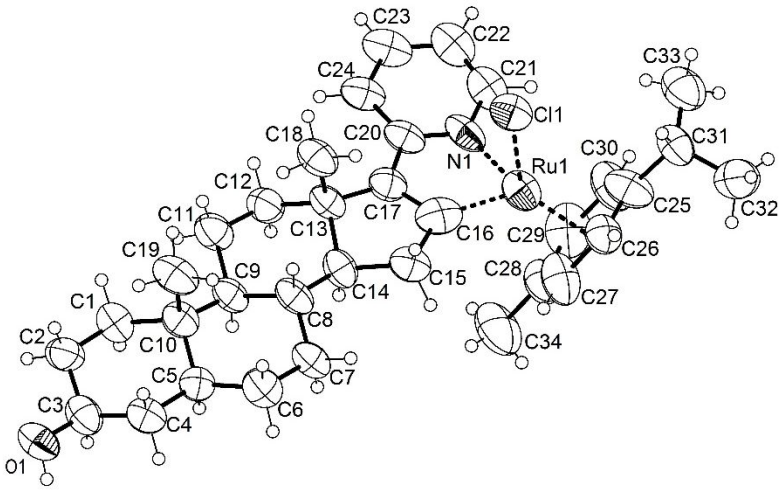


**Figure 4:** Molecular structure of the 2-pyridinyl ruthenium(II) complex **(*R*-Ru)-8** (displacement parameters are drawn at 50% probability level). Characteristic bond lengths: Ru–N 2.078(10) Å; Ru–C 1.931 Å; Ru–Cl 2.415(3) Å; Ru–cymene 2.130(16)–2.341(14) Å; Ru–cymene/centroid 1.729 Å. Selected bond angles: N–Ru–C 76.3(4)°, N–Ru–Cl 85.2(2)°, Cl–Ru–C 86.4(3)°, N–Ru–cymene$^{centroid}$ 132.33°, Cl–Ru–cymene$^{centroid}$ 126.60°, C–Ru–cymene$^{centroid}$ 130.34°.

Furthermore, comparable iridium(III) complexes were synthesized by applying similar reaction conditions and $[IrCp^*Cl_2]_2$ as metal precursor. The three cyclometalated Ir(III) complexes **9**, **10** and **11** (Scheme 3) were synthesized in overall good yields whereby the diastereomers of **10** and **11** were formed in equal amounts giving two sets of signals in the $^1H$ and $^{13}C$ NMR spectra. Unfortunately, a separation of the diastereomers **11** *via* column chromatography was not successful.

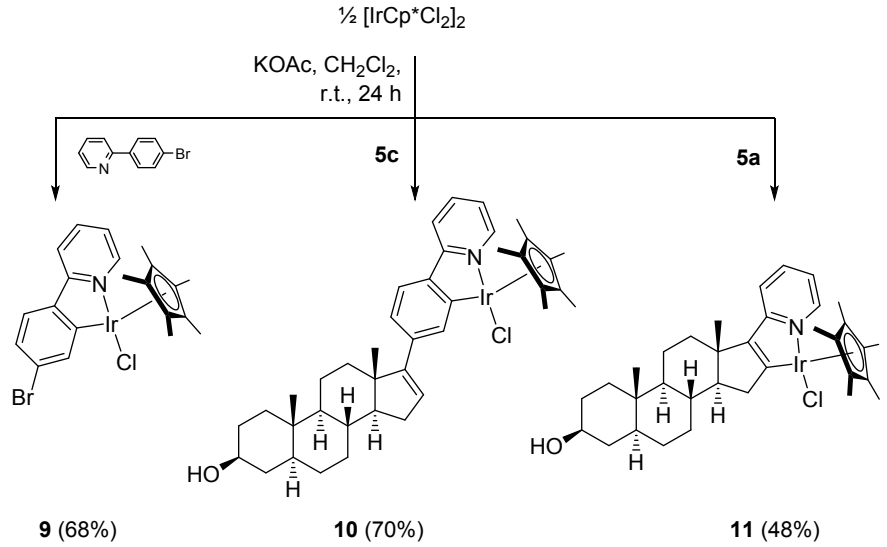


**Scheme 3:** Synthesis of novel cyclometalated iridium(III) complexes **9**, **10** and **11**.

For comparison with the cycloruthenated complexes **7** and **8** as well as for the analogous iridium(III) complexes **10** and **11**, (17-(3'-pyridinyl)androsten)dichloride ruthenium(II) complex **12** and the corresponding iridium(III) complex **13** were synthesized by stirring two equivalents of the ligand **5b** and one equivalent of the dimeric metal precursor in dichloromethane (Scheme 4). After precipitation with *n*-hexane, the metal complexes **12** and **13** were obtained in good yields.

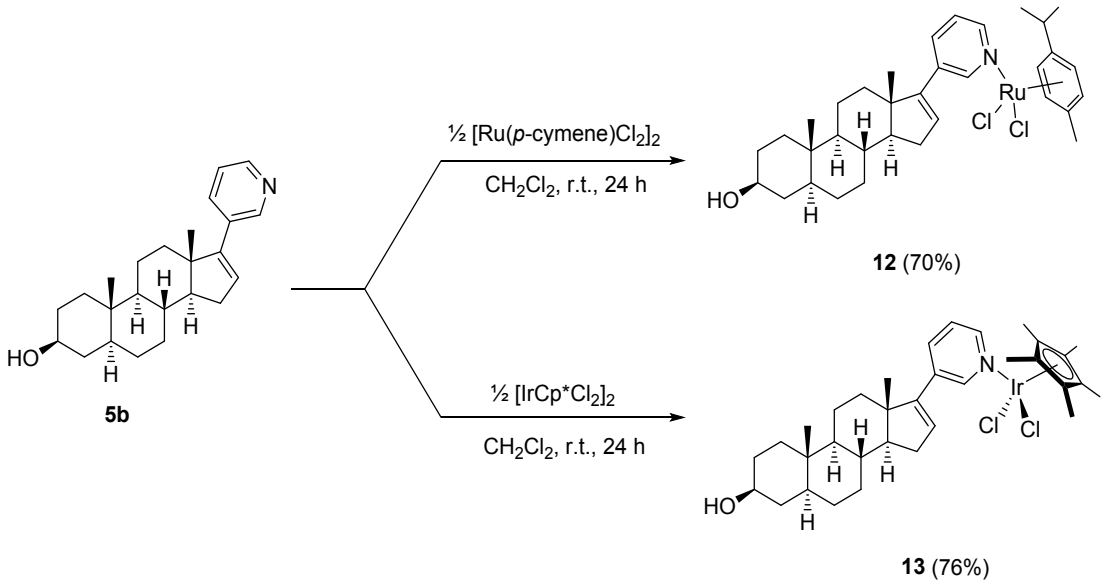

**Scheme 4:** Synthesis of the (17-(3′-pyridinyl)androstenido)dichloride ruthenium(II) complex **12** and the corresponding irdium(III) complex **13**.

We were able to obtain crystal structures suitable for crystal structure analysis for both 3-pyridyl complexes **12** and **13** (Figure 5) confirming their molecular structure and the pseudo-tetrahedral coordination geometry around the metal. Interestingly, in the solid state the nitrogen atom of the pyridyl moiety points towards the 18-methyl group and the metal atoms were located on the upper side of the steroidal framework. It is noteworthy that the ruthenium(II) complex **12** shows almost no distortion (6.81°) in contrast to the free ligand **5b** (see Supporting Information for the crystal structure) and the iridium(III) complex **13** whose pyridine units are twisted to the D-ring plane with a torsion of 32.9(3)° or 29.1(8)°.

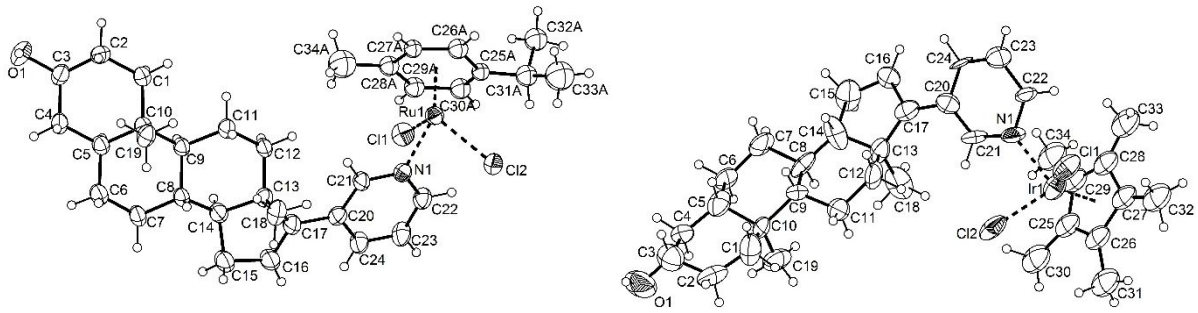


**Figure 5:** Molecular structure of the 3-pyridyl ruthenium(II) complex **12** (left) and the 3-pyridyl irdium(III) **13** (right). The cymene ligand of ruthenium(II) complex **12** is disordered. Selected bond lengths for **12**//**13**: Ru–N 2.125(3) Å; Ru–$C^{cymene}$ 2.159(10)–2.231(10) Å; Ru–$Cl^1$ 2.419 Å; Ru–$Cl^2$ 2.404 Å // Ir–$Cl^1$ 2.395(5) Å; Ir–$Cl^2$ 2.408(6) Å; Ir–N 2.090(5) Å; Ir–$C^{Cp*}$ 2.11(2)–2.26(2) Å; Ir–$C^{cymene/centroid}$ 1.788 Å. Selected bond angles for **12**//**13**: $Cl^1$–Ir–$Cl^2$ 89.2(2)°; N–Ir–$Cl^1$

85.9(5)°; N–Ir–$Cl^2$ 85.6(5)°; N–Ir–$cymene^{centroid}$ 125.7(2)°; $Cl^1$–Ir–$cymene^{centroid}$ 127.4(8)°; $Cl^2$–Ir–$cymene^{centroid}$ 128.9(5)° // $Cl^1$–Ru–$Cl^2$ 87.4(7)°; N–Ru–$Cl^1$ 85.2(1)°; N–Ir–$Cl^2$ 84.9(0)°.

**Biological Activity and Cytotoxicity Studies**

To evaluate the cytotoxicity of the compounds an *in vitro* MTT assay was performed (Table 2). The MTT (3-(4,5-dimethylthiazol-2-yl)-2,5-diphenyltetrazolium bromide) reagent can be reduced to blue-purple formazan by the mitochondrial enzymes of living cells. The amount of the resulting formazan can be determined photometrically and correlates directly with the cell viability, since this reaction can only take place in metabolically active cells. Therefore, the human bladder carcinoma cell line RT112 and its cisplatin resistant counterpart RT112cp were cultivated with varying concentrations (0.5 – 50 µM) of the ruthenium(II)- (**6**, **7**, **8** and **12**) and iridium(III)-complexes (**9**, **10**, **11** and **13**) and the cell viability was monitored after 72 h of incubation. In addition, cytotoxicity of the free ligands (**1**, **5a**-**c**) and cisplatin was evaluated for comparison. All complexes demonstrated higher cytotoxicity against RT112cp cells compared to cisplatin ($LD_{50}$ values 1 – 11 µM and > 50µM, respectively). The toxicity of the complexes **8**, **11**, **12** and **13** is similar to that of the corresponding free steroidal ligands (**5a** and **5b**), which

were shown to toxic in both cell lines with $LD_{50}$ values in the range between 2.5 and 7.5 μM. However, the steroidal ligand **5c** demonstrated high biocompatibility ($LD_{50}$ > 50 μM for both cell lines), whereas the corresponding Ru(II) (**7**) and Ir(III) (**10**) complexes showed promising antiproliferative effect in both cell lines. This indicates the cisplatin resistance was successfully overcome with $LD_{50}$ values of 1 μM for RT112cp cells and very low resistance factors of 0.33 and 0.5, respectively. Although the nonsteroidal complexes **6** and **9** were also more toxic ($LD_{50}$ 5 – 8 μM) compared to the free nonsteroidal ligand **1** ($LD_{50}$ > 50 μM), the steroidal complexes **7** and **10** were significantly more effective with considerably lower $LD_{50}$ values and resistance factors.

**Table 2:** $LD_{50}$ values and resistance factors (RF, $LD_{50(resistant)}/LD_{50(sensitive)}$) of the Ru(II)- and Ir(III)-complexes, free ligands and cisplatin (μM).

| Entry | Compound | RT112 | RT112cp (RF) |
|---|---|---|---|
| 1 | 2-Phenylpyridine | >50 | >50 |
| 2 | Ru(II)-complex **6** | 5 | 5 (1) |
| 3 | Ir(III)-complex **9** | 7.5 | 8 (1.07) |
| 4 | Ligand **5a** | 2.5 | 2 (0.8) |
| 5 | Ru(II)-complex **8** | 4 | 3 (0.75) |
| 6 | Ir(III)-complex **11** | 4.5 | 2.5 (0.56) |
| 7 | Ligand **5b** | 7.5 | 7 (0.93) |
| 8 | Ru(II)-complex **12** | 9 | 7.5 (0.83) |
| 9 | Ir(III)-complex **13** | 9 | 11 (1.22) |
| 10 | Ligand **5c** | >50 | >50 |
| 11 | Ru(II)-complex **7** | 3 | 1 (0.33) |
| 12 | Ir(III)-complex **10** | 2 | 1 (0.5) |
| 13 | Cisplatin | 3.5 | >50 |

## Conclusion

In conclusion, a set of Ru(II)- and Ir(III)-complexes with different *N*-containing ligands based on a steroidal backbone were synthesized and characterized by NMR spectroscopy and X-ray crystallography. All evaluated complexes showed high cytotoxicity in both RT112 and RT112cp (cisplatin-resistant) cell lines and were more active in RT112cp cells than cisplatin. Remarkable is the very low resistant factor of the complexes in the range between 0.33 and 1.22, indicating successful overcoming of the cisplatin resistance. Especially promising results were obtained for the complexes **7** and **10** with the steroidal ligand **5c,** since the advantageous high biocompatibility of **5c** ($LD_{50}$ > 50 μM) was combined with a pronounced antiproliferative effect of the complexes **7** ($LD_{50}$ 3 μM for RT112 and 1 μM for RT112cp) and **10** ($LD_{50}$ 2 μM for RT112 and 1 μM for RT112cp) with resistant factors 0.33 and 0.5, respectively.

## Experimental Section

**Instrumental Measurements:** ATR IR spectra were performed on Bruker alpha-p and a FT-IR IFS 88 spectrometer. $^{1}H$ and $^{13}C$ NMR spectra were recorded on different types of *Bruker* Avance

400, *Bruker* Avance III HD, or *Bruker* Avance 600 spectrometer with residual proton signals of the deuterated solvent as internal standard. EI and FAB mass spectra (positive mode) were measured on a Finnigan MAT95. Further information are given in the supporting information.

**General procedure for metallacyclisation reactions with ruthenium(II) and iridium(III):** Under argon atmosphere, the ligand (2.00 equiv.), $[RuCl_2(p\text{-cymene})]_2$ (1.00 equiv.) or $[IrCp^*Cl_2]_2$ (1.00 equiv.) and KOAc (4.00 equiv.) were dissolved in dry MeOH or $CH_2Cl_2$ and stirred at r.t. for 24 h. The suspension was concentrated and the residue was purified by flash column chromatography on silica gel to obtain the cyclometalated complexes as yellow to orange solids. The reactions based on a steroidal ligand were performed on a 30 – 120 µmol scale.

**Crystal structure determinations**

The single-crystal X-ray diffraction study of **5b**[15] and **7** was carried out on a Bruker D8 Venture diffractometer with Photon100 detector at 123(2) K using Cu-K$\alpha$ radiation ($\lambda$ = 1.54178 Å). Direct Methods (SHELXS-97)[24] was used for structure solution and refinement was carried out using SHELXL-2014 (full-matrix least-squares on $F^2$)[25]. Hydrogen atoms were localized by difference electron density determination and refined using a riding model (H(O) free). A semi-empirical absorption corrections were applied. The absolute configuration were determined by refinement of Parsons' x-parameter[26]. The single-crystal X-ray diffraction study of **(*R*-Ru)-8**, **12** and **13** was performed on a *Stoe StadiVari* diffractometer using Ga-Kα radiation (λ = 1.34143 Å) generated by an Metaljet X-ray source. The crystals were kept at 180.15 K during data collection. Using

Olex2[27], the structures were solved with the ShelXS[24] structure solution program using Direct Methods and refined with the ShelXL[25] refinement package using Least Squares minimization. Non-hydrogen atoms were refined with anisotropic displacement parameters; hydrogen atoms were modelled on idealized positions.

CCDC 1521243 (**5b**), 1859054 (**7**), 1944097 ((***R*-Ru)-8**), 1944098 (**12**) and 1944099 (**13**) contain the supplementary crystallographic data for this paper. These data can be obtained free of charge from the Cambridge Crystallographic Data Centre *via* www.ccdc.cam.ac.uk/data_request/cif.

**Computational Details**

Structure optimizations were done on the BP86[17]/def2-TZVPP[18] level of theory using the TURBOMOLE 7.1 program package.[28] Solvent effects of Chloroform were taken into account with the COSMO solvation model.[29] The RI-approximation was used throughout.[30] Stationary points were verified to be minimum energy structures by numerically calculating the molecular Hessian and analyzing the so obtained vibrational frequencies. The numerical frequencies were used to calculate thermodynamic properties at 298.15 K and 1 bar in harmonic and ideal gas approximations. NMR chemical shifts were calculated on the basis of Gauge Including Atomic Orbitals (GIAO).[31]

**Cell Culture**

RT112 (human bladder carcinoma cell line) and RT112cp (cisplatin-resistant) cells were cultured with RPMI (Roswell Park Memorial Istitute) medium (Gibco) supplemented with 10% fetal bovine serum (FBS, Gibco) and 1% penicillin/streptavidin (Gibco) at 37 °C, 5% $CO_2$, and humid atmosphere. For all *in vitro* experiments, cells were trypsinized (0.05% trypsin-EDTA, Gibco) and seeded in 96-well-plates (toxicity assay) at the required densities. Incubation was performed under the culture conditions as described above.

**Cytotoxicity Assay**

RT112 (human bladder carcinoma cell line) and RT112cp (cisplatin-resistant) cells were seeded in the 96-well-plates at a density of $1x10^4$ cells/well in RPMI medium supplemented with 10% FCS and 1% penicillin/streptomycin. After 24 h of incubation at 37 °C, 5% $CO_2$, the medium was removed and the cells were treated with various concentrations of the compounds in RPMI medium (DMSO concentration < 0.5%) and incubated for 72 h at 37 °C, 5% $CO_2$. As a negative control, the cell culture medium was exchanged without addition of the compounds. Thereafter, 15 µl of the MTT reagent (Promega) were given in each well. For the positive control, Triton X-100 (1%) was added

in some wells before treating them with the MTT reagent. After 3 h of incubation the cells were lysed using the Stop Solution (Promega) to release the blue-purple formazan. The cell viability was determined by measuring the absorbance of the resulting formazan at 595 nm using a multiwell plate reader (SpectraMax ID3, Molecular Devices, USA) and calculated in relation to the negative control.

**Acknowledgements**

We thank the Complat platform for managing and transferring the compounds. V.K. gratefully acknowledges the Studienstiftung des Deutschen Volkes and W.F. the Carl-Zeiss-Stiftung for financial support. The work was supported by the Deutsche Forschungsgemeinschaft (DFG), within the Research Training Group 2039 (A.M., U.S. S.B.) and the Helmholtz Program Biointerfaces in Technology and Medicine (BIFTM) (U.S., A.M., S.B.). We thank Prof. Dr. Frank Breher for supporting this cooperation.

**References**

[1] F. Le Bideau, S. Dagorne, *Chem. Rev.* **2013**, *113*, 7793-7850.

[2] J. J. Wilson, S. J. Lippard, *Chem. Rev.* **2014**, *114*, 4470-4495.

[3] a) B. Rosenberg, L. Van Camp, T. Krigas, *Nature* **1965**, *205*, 698; b) B. V. C. Rosenberg, Loretta; Grimley, Eugene B.; Thomson, Andrew J., *J. Biol. Chem.* **1967**, *242*, 1347-1352.

[4] a) S. Faivre, D. Chan, R. Salinas, B. Woynarowska, J. M. Woynarowski, *Biochem. Pharmacol.* **2003**, *66*, 225-237; b) E. Raymond, S. G. Chaney, A. Taamma, E. Cvitkovic, *Ann. Oncol.* **1998**, *9*, 1053-1071.

[5] W. H. Ang, A. Casini, G. Sava, P. J. Dyson, *J. Organomet. Chem.* **2011**, *696*, 989-998.

[6] F. Lentz, A. Drescher, A. Lindauer, M. Henke, R. A. Hilger, C. G. Hartinger, M. E. Scheulen, C. Dittrich, B. K. Keppler, U. Jaehde, i. c. w. C. E. S. f. A. D. Research-EWIV, *Anti-Cancer Drugs* **2009**, *20*, 97-103.

[7] E. Alessio, *Eur. J. Inorg. Chem.* **2017**, *2017*, 1549-1560.

[8] a) J. M. Rademaker-Lakhai, D. van den Bongard, D. Pluim, J. H. Beijnen, J. H. M. Schellens, *Clin Cancer Res.* **2004**, *10*, 3717-3727; b) C. G. Hartinger, M. A. Jakupec, S. Zorbas-Seifried, M. Groessl, A. Egger, W. Berger, H. Zorbas, P. J. Dyson, B. K. Keppler, *Chem. Biodivers.* **2008**, *5*, 2140-2155; c) S. Leijen, S. A. Burgers, P. Baas, D. Pluim, M. Tibben, E. van Werkhoven, E. Alessio, G. Sava, J. H. Beijnen, J. H. M. Schellens, *Invest. New Drugs.* **2015**, *33*, 201-214.

[9] a) M. V. Babak, S. M. Meier, K. V. M. Huber, J. Reynisson, A. A. Legin, M. A. Jakupec, A. Roller, A. Stukalov, M. Gridling, K. L. Bennett, J. Colinge, W. Berger, P. J. Dyson, G. Superti-Furga, B. K. Keppler, C. G. Hartinger, *Chem. Sci.* **2015**, *6*, 2449-2456; b) G. Gasser, I. Ott, N. Metzler-Nolte, *J. Med.Chem.* **2011**, *54*, 3-25; c) C. G. Hartinger, N. Metzler-Nolte, P. J. Dyson, *Organometallics* **2012**, *31*, 5677-5685.

[10] L. Simeone, G. Mangiapia, G. Vitiello, C. Irace, A. Colonna, O. Ortona, D. Montesarchio, L. Paduano, *Bioconjugate Chem.* **2012**, *23*, 758-770.

[11] a) S. Top, H. El Hafa, A. Vessières, M. Huché, J. Vaissermann, G. Jaouen, *Chem. Eur. J.* **2002**, *8*, 5241-5249; b) A. Vessières, S. Top, C. Vaillant, D. Osella, J.-P. Mornon, G. Jaouen, *Angew. Chem. Int. Ed.* **1992**, *31*, 753-755.

[12] a) M. Huxley, C. Sanchez-Cano, M. J. Browning, C. Navarro-Ranninger, A. G. Quiroga, A. Rodger, M. J. Hannon, *Dalton Trans.* **2010**, *39*, 11353-11364; b) C. Sanchez-Cano, M. Huxley, C. Ducani, A. E. Hamad, M. J. Browning, C. Navarro-Ranninger, A. G. Quiroga, A. Rodger, M. J. Hannon, *Dalton Trans.* **2010**, *39*, 11365-11374; c) C. Sanchez-Cano, M. J. Hannon, *Dalton Trans.* **2009**, 10765-

10773; d) A. Jackson, J. Davis, R. J. Pither, A. Rodger, M. J. Hannon, *Inorg. Chem.* **2001**, *40*, 3964-3973.

[13] a) J. Ruiz, V. Rodriguez, N. Cutillas, K. G. Samper, M. Capdevila, O. Palacios, A. Espinosa, *Dalton Trans.* **2012**, *41*, 12847-12856; b) J. Ruiz, V. Rodríguez, N. Cutillas, A. Espinosa, M. J. Hannon, *Inorg. Chem.* **2011**, *50*, 9164-9171.

[14] a) A. J. Millett, A. Habtemariam, I. Romero-Canelón, G. J. Clarkson, P. J. Sadler, *Organometallics* **2015**, *34*, 2683-2694; b) Z. Liu, A. Habtemariam, A. M. Pizarro, S. A. Fletcher, A. Kisova, O. Vrana, L. Salassa, P. C. A. Bruijnincx, G. J. Clarkson, V. Brabec, P. J. Sadler, *J. Med.Chem.* **2011**, *54*, 3011-3026; c) Z. Liu, A. Habtemariam, A. M. Pizarro, G. J. Clarkson, P. J. Sadler, *Organometallics* **2011**, *30*, 4702-4710.

[15] V. Koch, M. Nieger, S. Bräse, *Adv. Synth. Catal.* **2017**, *359*, 832-840.

[16] a) B. Li, C. Darcel, T. Roisnel, P. H. Dixneuf, *J. Organomet. Chem.* **2015**, *793*, 200-209; b) I. Özdemir, S. Demir, B. Çetinkaya, C. Gourlaouen, F. Maseras, C. Bruneau, P. H. Dixneuf, *J. Am. Chem. Soc.* **2008**, *130*, 1156-1157; c) E. Ferrer Flegeau, C. Bruneau, P. H. Dixneuf, A. Jutand, *J. Am. Chem. Soc.* **2011**, *133*, 10161-10170.

[17] a) A. D. Becke, *Phys. Rev. A* **1988**, *38*, 3098-3100; b) J. P. Perdew, *Phys. Rev. B* **1986**, *33*, 8822-8824.

[18] F. Weigend, R. Ahlrichs, *Phys. Chem. Chem. Phys.* **2005**, *7*, 3297-3305.

[19] J. Kim, J. Kim, S. Chang, *Chem. Eur. J.* **2013**, *19*, 7328-7333.

[20] J.-P. Djukic, A. Berger, M. Duquenne, M. Pfeffer, A. de Cian, N. Kyritsakas-Gruber, J. Vachon, J. Lacour, *Organometallics* **2004**, *23*, 5757-5767.

[21] J. Tao, J. P. Perdew, V. N. Staroverov, G. E. Scuseria, *Phys. Rev. Lett* **2003**, *91*, 146401.

[22] J. B. Lambert, E. P. Mazzola, *Nuclear Magnetic Resonance Spectroscopy: An Introduction to Principles, Applications, and Experimental Methods*, Pearson Education, **2004**.

[23] The only examples in the literature are complexes of the type $L_2RuCl$ ($\eta^2$-$CH{=}CHC_5H_4N$) (e.g. L = $(P^iPr_3)_2$) and $L_2ClH_nRu(\eta^2$-‡$C(D){=}CR(EWG)$: a) J. N. Coalter, W. E. Streib, K. G. Caulton, *Inorg. Chem.* **2000**, *39*, 3749-3756; b) L.

Zhang, L. Dang, T. B. Wen, H. H. Y. Sung, I. D. Williams, Z. Lin, G. Jia, *Organometallics* **2007**, *26*, 2849-2860.

[24] G. Sheldrick, *Acta Crystallogr. A* **2008**, *64*, 112-122.

[25] G. Sheldrick, *Acta Crystallogr. C* **2015**, *71*, 3-8.

[26] S. Parsons, H. D. Flack, T. Wagner, *Acta Crystallogr. B* **2013**, *69*, 249-259.

[27] O. V. Dolomanov, L. J. Bourhis, R. J. Gildea, J. A. K. Howard, H. Puschmann, *J. Appl. Cryst.* **2009**, *42*, 339-341.

[28] TURBOMOLE V7.1 2016, 1989-2007, TURBOMOLE GmbH, since 2007; available from http://www.turbomole.com.

[29] A. Klamt, G. Schuurmann, *J. Chem. Soc., Perkin Trans. 2* **1993**, 799-805.

[30] M. Sierka, A. Hogekamp, R. Ahlrichs, *J. Phys. Chem .* **2003**, *118*, 9136-9148.

[31] G. Schreckenbach, T. Ziegler, *J. Phys. Chem.* **1995**, *99*, 606-611.

TOC:

Cyclometallated- and pyridyl ruthenium(II)- and iridium(III)-complexes conjugated to the steroidal backbone *epi*-androsterone were synthesized and their cytotoxic properties in RT112 and RT112cp (cisplatin resistant) cell lines were investigated.